ELSEVIER

Contents lists available at ScienceDirect

Nano Today

journal homepage: www.elsevier.com/locate/nanotoday





Investigating the influence of particle hydrophobicity on lung deposition using nonionic dye partitioning

Guangle Li a,1 , Zheng Dong b,c,f,1 , Quanzhong Ren b,d , Bingbing Sun e , Sijin Liu b,c,f , Juan Ma b,c,* , Yi Y. Zuo a,g,**

- ^a Department of Mechanical Engineering, University of Hawaii at Manoa, Honolulu, HI 96822, United States
- b State Key Laboratory of Environmental Chemistry and Ecotoxicology, Research Center for Eco-Environmental Sciences, Chinese Academy of Sciences, Beijing 100085, China
- ^c University of Chinese Academy of Sciences, Beijing 100049, China
- d Department of Toxicology and Sanitary Chemistry, School of Public Health, Capital Medical University, Beijing 100069, China
- ^e State Key Laboratory of Fine Chemicals, Dalian University of Technology, Dalian 116024, China
- f Medical Science and Technology Innovation Center, Shandong First Medical University & Shandong Academy of Medical Sciences, Jinan, Shandong 250117, China
- g Department of Pediatrics, John A. Burns School of Medicine, University of Hawaii, Honolulu, HI 96826, United States

ARTICLE INFO

Keywords: Particulate matter Hydrophobicity Dye partitioning Lung deposition Rhodamine B

ABSTRACT

The regional deposition of inhaled particulate matter (PM) in the respiratory tract determines its biological fate and lung toxicity. While it is widely accepted that the size of PM plays a predominant role in affecting lung deposition, the impact of other physicochemical properties, especially hydrophobicity, remains unclear. This knowledge gap exists, in part, due to the absence of standard methods to characterize the hydrophobicity of PM. Here, we developed a novel nonionic dye partitioning method to quantitatively characterize the hydrophobicity of PM. The use of a nonionic dye, rhodamine B, effectively eliminates experimental artifacts arising from unwanted dye adsorption due to electrostatic interactions, thus significantly improving the accuracy and applicability of the method. Through an intranasal mouse exposure model, we discovered that the lung deposition of four types of PM originated from common anthropogenic sources, including PM2.5, dust, biochar, and carbon black, is mediated by their hydrophobicity. The most hydrophobic PM tends to be trapped in the nasal cavity, whereas the least hydrophobic PM penetrates deep into the alveoli, inducing severe lung inflammation. The hydrophobicity-dependent deposition of PM in the respiratory tract offers novel insights into understanding the acute lung toxicity of inhaled PM and provides a foundation for the design of safer and more efficacious inhalable medicines. Furthermore, the nonionic dye partitioning method shows promise as a user-friendly and cost-effective approach for characterizing the hydrophobicity of PM.

Introduction

Airborne particulate matter (PM) is a global environmental pollutant that poses a significant threat to public health[1,2]. The source of airborne PM is mainly attributed to human activities, such as coal/oil combustion, biomass burning, traffic emissions, and diverse industrial activities[1,2]. Numerous epidemiological and toxicological studies have revealed the adverse health impact of human exposure to airborne PM *via* inhalation, ingestion, or dermal penetration[3–6]. It was found that exposure to airborne PM is correlated with increased incidence of

skin, respiratory and cardiovascular diseases, as well as elevated morbidity and mortality of various cancers[7,8]. Among all possible exposure portals, the respiratory system appears to be the most susceptible to airborne PM, because of its large surface area in direct contact with the environment[9]. Regional deposition of inhaled PM in the respiratory system is influenced by various physicochemical properties of the PM, including its aerodynamic size, density, shape, charge, hydrophobicity, and hygroscopicity[10,11]. The deposition region of the PM further determines its lung toxicity and biological fate, e.g., mucociliary clearance and mucosal penetration for particles deposited in the

^{*} Correspondence to: Department of Mechanical Engineering, University of Hawaii at Manoa, 2540 Dole St, Holmes Hall 302, Honolulu, HI 96822, United States.

^{**} Correspondence to: No.18. Shuangqing Road, Haidian District, Beijing 100085, China. *E-mail addresses*: juanm@rcees.ac.cn (J. Ma), yzuo@hawaii.edu (Y.Y. Zuo).

¹ These authors contributed equally to this work.

airway[12], or macrophage clearance, endocytosis, and translocation for particles penetrating deep into the alveolar region[9,11,13].

Although it is generally accepted that the size of PM is the most predominant factor that determines its lung deposition[14,15], there is strong evidence that the hydrophobicity of PM also plays a significant role in mediating lung deposition[6,16–18]. Nevertheless, in comparison to numerous studies of particle size-dependent deposition, it is still largely unknown how the hydrophobicity of PM affects its lung deposition. This knowledge gap could be in part due to technical difficulties in quantitatively characterizing the hydrophobicity of PM. Multiple methods have been developed to characterize the hydrophobicity of PM, such as the contact angle method[19], capillary penetration[20], two-phase partitioning[21,22], dye partitioning[21,23,24], inverse gas chromatography[25], and maximum particle dispersion[26,27]. All these methods have technical limitations[27]. A reliable and standard method for characterizing the hydrophobicity of PM is still lacking.

Among all available methods, dye partitioning stands out as an easyto-use and low-cost method to characterize the hydrophobicity of PM. In this method, a hydrophobic dye, such as rose bengal (RB)[23], is mixed with the PM at a series of predetermined concentrations. The relative hydrophobicity of different PMs is determined by plotting the partitioning quotient (PQ) of the dve, defined as the ratio of the dve bound onto the PM surface to the free dye in the liquid phase, against the total surface area of the dispersed PM at various particle concentrations[28]. A hydrophobic dye is expected to have more of its molecules bound to the surface of a more hydrophobic PM, indicated by a larger PQ slope. Similarly, when a hydrophilic dye, such as nile blue (NB)[21], is used, the PM with a larger PQ slope represents a higher hydrophilicity, i.e., lower hydrophobicity. Although being a seemingly straightforward method, current dye partitioning method has an intrinsic mechanistic flaw, i.e., the adsorption of dye molecules onto the particle surfaces is not only determined by hydrophobic interactions but also by electrostatic interactions[27]. Consequently, the experimentally measured PQ is a combined result of hydrophobic and electrostatic interactions between the PM and the dye. Since RB is negatively charged and NB is positively charged, while most PM dispersed in the aqueous phase carries a net negative charge, the RB partitioning method tends to underestimate the hydrophobicity, while the NB partitioning method tends to overestimate the hydrophilicity. This experimental flaw of the dye partitioning method can be somehow mitigated by taking ratios between the hydrophobicity measurement with RB and the hydrophilicity measurements with NB[24]. Nevertheless, the current dye partitioning method is only feasible in characterizing particles with extreme hydrophobicity but largely fails for moderately hydrophobic particles.

To decouple dye adsorption due to the hydrophobic interaction from that due to the electrostatic interaction, here we propose to use a nonionic dye, rhodamine B (RhB), to characterize the hydrophobicity of PM. We have studied four representative PMs that cover the primary anthropogenic sources of PMs[6]. These are PM2.5 collected from the atmospheric environment, dust particles mainly composed of silicon dioxide, biochar particles resulted from biomass burning, and carbon black particles collected from exhausts of natural gas combustion. Using an intranasal mouse exposure model, we have established the correlation between the hydrophobicity of the PMs and their regional deposition in the respiratory tract.

Materials and methods

Particulate matter

Carbon black particles were obtained from Degussa Inc. (USA). Biochar particles were prepared via pyrolyzing biomass from corn straw under oxygen-limited conditions at 500 °C, as described previously [29]. The biochar powder was crushed and passed through a 3- μ m sieve. Dust was purchased from Powder Technology Inc. (USA). Airborne PM2.5 samples were collected in Beijing, China. Elemental composition of the

PM was determined with energy-dispersive X-ray spectroscopy (Hitachi, Japan). Primary size of the PM was determined with scanning electron microscopy (Hitachi, Japan). Aerodynamic size of the airborne PM was determined with an aerodynamic particle sizer (TSI APS 3321, USA). Zeta potential of the PM in aqueous environment with a pH of 7.4 was determined with Zetasizer (Malvern Panalytical, UK).

Dyes

Rose bengal (RB), nile blue (NB), and rhodamine B (RhB) were purchased from Sigma-Aldrich and used without further purification. As shown in Table 1 and Figure S1, RB is negatively charged (pKa = 1.89), while NB is positively charged (pKa = 10.0)[30,31]. In contrast, RhB is a weakly water-soluble, zwitterionic, hydrophobic dye. Similar to RB, the hydrophobicity of RhB originates from its xanthene moiety. Owing to its remarkable photophysical properties, such as the high absorption coefficient, high fluorescence quantum yield, and photostability, RhB has been extensively used as a fluorescent probe [32-34]. RhB is sensitive to the solvent environment because of its phenyl carboxylic group. It can exist as protonated, zwitterionic, or colorless lactone forms[35-39]. In water and alcohols. RhB primarily exists as a zwitterion, which is deeply colored[35]. The pKa of RhB is 3.2, indicating that in a neutral aqueous environment with a pH of 7.4, RhB exists in a zwitterionic form[39]. In this form, the positive and negative charges within the RhB solution are largely balanced, giving rise to an overall neutral charge and highlighting its nonionic nature. Other nonionic dyes, such as Eosin Y, have low pKa values, making them negatively charged under the neutral pH conditions[40], and hence are incapable of serving as an appropriate zwitterionic dye for hydrophobicity measurements.

Previous research has demonstrated that the adsorption of RhB in its zwitterionic form to negatively charged polyelectrolytes is considerably lower compared to its protonated counterpart[41]. In neutral water, RhB exhibits a prominent absorption band at 554 nm, representing the highly colored zwitterionic form. This absorption remains relatively constant within the pH range of 7.0–12.0[39]. Figure S2 shows that the absorption peak of RhB is at 554 nm, indicating the zwitterion form of RhB

Dye partitioning methods for characterizing the hydrophobicity of PM

Description of the rose bengal and nile blue partitioning methods can be found elsewhere [24]. For the nonionic dye partitioning method, rhodamine B (RhB) was dissolved in water to a concentration of 1 mg/mL, with vortex and sonication, and then diluted to 20 μg/mL using the PBS solution. A series of PM stock solutions were added to the dye solution to create a battery of the dye-PM suspensions. Controls were prepared by adding the same volume of the dispersion liquid to the dye solution to account for the slightly increased volume due to the addition of the stock solution. All suspensions were incubated at room temperature for 90 min and subsequently centrifuged at 16,000 g for 30 min. Supernatants were collected, and dye molecules in supernatants were analyzed with a UV-vis spectrometer (Epoch, BioTek) at 554 nm. The partitioning quotient (PQ) was calculated by the ratio of the dye bound onto the PM surface (Dbound) to free dye molecules in the liquid phase (D_{free}), i.e., $PQ = D_{bound}/D_{free}$. The total surface area of the PM dispersed in the suspension was calculated from the hydrodynamic size of the PM, by assuming a spherical shape. The PQ vs. the surface area of the PM was plotted, and the slope of the linear regression was obtained using OriginPro.

Maximum particle dispersion method

The maximum particle dispersion (MPD) method was implemented following established procedures [26,27]. In brief, a minute quantity of the PM stock solution was added to a series of probing liquids, each consisting of 0.5 mL. These probing liquids were composed of

Table 1
Summary of anionic (rose bengal), cationic (nile blue), and nonionic (rhodamine B) dyes used in dye partitioning method for characterizing the hydrophobicity or hydrophilicity of particles.

Dye	Rose bengal	Nile blue	Rhodamine B
Chemical structure (with the functional groups highlighted)	CI CI ONA	0 0 0 0 0 0 0 0 0 0 0 0 0 0 0 0 0 0 0	H ₃ C N CH ₃
Chemical formula	$C_{20}H_2Cl_4I_4Na_2O_5$	$2 C_{20}H_{20}N_3O \cdot SO_4$	$C_{28}H_{30}N_2O_3$
Molar mass (g/mol)	1017.64	732.85	442.55
Charge	Anionic	Cationic	Nonionic/Zwitterionic
pKa	3.93/1.89 [30] ^a	10.0 [31]	3.2 [39] ^b
Hydrophobic / hydrophilic group	Xanthene ring (hydrophobic)	Amino group (hydrophilic)	Xanthene ring (hydrophobic)
Peak λ _{absorbance} (nm)	549	635	554
Water solubility	Soluble	Soluble	Weakly soluble

^a pK_a of 3.93 and 1.89 are attributed to the hydroxyl group and the carboxylic group, respectively.

water/ethanol mixtures, effectively covering a surface tension range between 21.4 and 71.9 mJ/m². The mixtures were thoroughly vortexed to ensure homogeneity, followed by a 30-minute period of natural sedimentation and subsequent centrifugation at 100 g for 5 minutes to facilitate particle sedimentation, except for the dust particles that required only natural sedimentation. Subsequently, 160 µL of the supernatant from each suspension was carefully transferred to individual wells of a 96-well microplate, ensuring that the sediment was undisturbed. The optical density at 400 nm (OD400) was determined using a microplate reader (Epoch, BioTek). The optical density data was then plotted against the surface tensions of the probing liquids. The surface free energy of the PM was determined by identifying the maximum optical density value, achieved through optimal peak fitting using OriginPro. To ensure reproducibility, each measurement was replicated at least three times, and the outcomes were presented as mean values \pm standard deviation.

Animal exposure experiments

The animal experimental protocols were approved by the Animal Ethics Committee at the Research Center for Eco-Environmental Sciences, Chinese Academy of Sciences (approval number: AEWC-RCEES-2020001). BALB/c mice (female, 6-7 weeks old) were obtained from the Vital River Laboratory Animal Technology Co. Ltd (Beijing, China), and were housed and maintained in a specific pathogen-free (SPF) facility. The mice were randomly divided into different groups and intranasally administrated with PM2.5, dust, biochar, and carbon black, respectively, at a dose of 1 mg/kg or 200 µg/kg bodyweight. Afterwards, the nasal cavity, trachea, and lung tissues were collected and fixed in 4 % paraformaldehyde for hematoxylin and eosin (H&E) staining. The integrated density (area × mean intensity) of differential PM deposition in the H&E-stained tissue sections was determined with ImageJ (National Institutes of Health, USA)[42,43]. The cell subpopulation in lung tissues was determined by an Attune NxT flow cytometry platform (ThermoFisher, USA). In brief, the single-cell suspensions from lung tissues were prepared and stained with fluorescence-conjugated antibodies for flow cytometry analysis, as previously reported [44]. Detailed information about the antibodies was shown in Table S1. The peripheral blood was collected and analyzed with a hematology analyzer (Nihon Kohden, Japan).

Cell culture and cell viability assessment

Human bronchial epithelial cells (BEAS-2B cells) were purchased from the Shanghai Cell Bank of Type Culture Collection at the Chinese

Academy of Sciences. BEAS-2B cells were cultured in the bronchial epithelial cell medium (ScienCell, USA) with 1 % bronchial epithelial cell growth supplement at 37 $^{\circ}$ C, 5 % CO₂, supplemented with 100 U/mL penicillin/streptomycin. Cell viability was determined with the CellTiter-Glo Luminescent Cell Viability Assay (Promega, USA) according to the manufacturer's instruction.

SDS-PAGE gel electrophoresis

After incubation with 50 µg/mL PM for 24 h, interactions between cells and PMs were visualized with a fluorescence microscope (AXIO Scope.A1, Zeiss, Germany). Cells were further washed twice with PBS to remove extra PM unattached to the cells. These cells were lysed in RIPA lysate buffer (Solarbio Life Science, China) containing the protease inhibitor cocktail (Roche, Switzerland). SDS-PAGE gel electrophoresis was performed using a standard BD Mini Vertical Gel (10 cm \times 8 cm) with 10 loading wells. We used 4 % stacking gel as the loading substrate for the PM. Twenty microliters of the cell lysate samples were loaded onto the SDS-PAGE gel and electrophoresed at 120 V for 2 h. The gel was scanned using a ChemiDoc XRS+ System (Bio-Rad, USA). The integrated optical densitometry (IOD) of the PM band on the gel image was quantified using ImageJ. When performing SDS-PAGE, the volume of cell lysates applied to each well was controlled so that the total amount of protein remained the same.

Interactions between cells and the PM

After treatment with 50 $\mu g/mL$ PM for 24 h, BEAS-2B cells were extensively washed with PBS and fixed with the glutaraldehyde solution. Ultrathin sections of the cells were prepared and stained with 1 % lead citrate and 0.5 % uranyl acetate. Cellular localization and internalization of the PM was examined by transmission electron microscopy (TEM, Hitachi, Japan).

PM uptake by cells

To track particle localization and internalization, we prepared fluorescein isothiocyanate (FITC)-bovine serum albumin (BSA) labeled PM following experimental protocols detailed elsewhere[29,45]. Briefly, 1 mg of FITC-BSA (five FITC per BSA) (Solarbio, China) was dissolved in 1 mL of sterile water. 1.0 mg/mL PM was co-incubated with 1.0 mg/mL FITC-BSA overnight at room temperature. The mixtures were washed 3 times with cold PBS by centrifugation at 16,000 g for 30 min to remove free FITC-BSA. The collected pellets were resuspended in sterile water, and the concentration of FITC-BSA-conjugated PM was determined

b pKa of 3.2 indicates the equilibrium between zwitterionic and cationic forms of RhB in the aqueous environment.

through an ultraviolet spectrophotometer (Shimadzu, UV-3600, Kyoto, Japan).

Results

Characterization of the PM

We have characterized the PM used in this study. As illustrated in Figure S3, both PM2.5 and dust primarily consist of silicon dioxide (SiO₂), accompanied by various metal and carbon impurities. Biochar and carbon black particles are mostly composed of elemental carbon. As shown in Table 2, the primary size of the PM shows a heterogeneous distribution, spanning a wide range from 20 nm to 6 μ m. Nevertheless, the aerodynamic size of the airborne PM exhibits a relatively uniform distribution, with PM2.5, biochar, and carbon black particles falling within the range of 1.2–1.46 μ m, and dust at 3.21 μ m. Zeta potential of the PM indicates that all particles carry a negative charge in the aqueous environment with a neutral pH of 7.4. Additional physicochemical properties of the PM are detailed in Table S2.

Determination of the PM hydrophobicity using the nonionic dye partitioning method $\,$

We first demonstrate the feasibility of the nonionic dye partitioning method by comparing to the classical RB (anionic dye) and NB (cationic dye) partitioning methods. Fig. 1 shows the comparison of different dye partitioning methods to characterize the hydrophobicity/hydrophilicity of the PM. As shown in Fig. 1A and B, out of four PMs, the PO slopes for RB partitioning of PM2.5, dust, and biochar are all near-zero, indicating negligible adsorption of the RB molecules onto these PMs. Therefore, the RB partitioning method only ranks the carbon black particles to be the most hydrophobic PM but is incapable of differentiating the hydrophobicity of the rest three PMs. Fig. 1C and D shows the results of NB partitioning, which ranks the hydrophilicity of these PMs as PM2.5 > dust > biochar > carbon black. The overall adsorption of NB is one to two orders of magnitude higher than the RB adsorption, indicating that unwanted electrostatic interactions contribute a significant portion of the dye adsorption. Fig. 1E and F shows the results of RhB partitioning, which ranks the hydrophobicity of the PMs as carbon black > biochar > dust > PM2.5. It appears that this ranking in particle hydrophobicity is in good agreement with the hydrophilicity ranking determined with the NB partitioning method. Nevertheless, the overall adsorption of NB is nearly two orders of magnitude greater than that of RhB (Fig. 1D vs. F), suggesting the possibility that undesired electrostatic attractions between this cationic dye and negatively charged particles might have played a predominant role in determining the NB adsorption.

We have verified the nonionic dye partitioning method using a completely independent method called the maximum particle dispersion (MPD)[26,27]. MPD is an optical technique used to quantitatively determine the surface free energy (SFE) of PM. This method hinges on a

unique measurement principle that quantifies the colloidal stability of PM suspensions by assessing the balance between van der Waals attraction and electrostatic repulsion [26,27]. As shown in Fig. 2, the SFE of these PMs was determined at 35.6 \pm 0.5, 33.7 \pm 0.5, 31.5 \pm 0.5, and 27.0 \pm 0.3 mJ/m² for PM2.5, dust, biochar, and carbon black, respectively. According to these SFE measurements, the hydrophobicity of these PMs can be ranked as PM2.5 < dust < biochar < carbon black, in good agreement with the particle hydrophobicity characterized by the nonionic dye partitioning method (Fig. 1F).

Hydrophobicity of the PM regulates its regional deposition in the lung

After characterizing the hydrophobicity of the PM used in this study, we have studied the regional deposition of these PMs in the respiratory tract. Aerodynamic sizes of these four PMs appear to be in the same order of magnitude, ranging from 1.2 to 3.2 μ m (Table 2). With a low-dose exposure model involving intranasal particle administration at 1 mg/kg bodyweight, only a limited number of particles can be detected in lung tissues[6]. Therefore, instead of relying on the particle count, we opted to utilize integrated density, calculated as the product of area and mean intensity of the PM using ImageJ. This method enables the quantification of aggregated and/or overlapped particles found within tissues[42,43]. Although the inherent color of these four types of PM varies slightly, the relative errors arising from color variations in assessing the integrated density of the PM in H&E-stained histological images were deemed negligible.

As shown in Fig. 3, it was found that carbon black, i.e., the most hydrophobic particle out of the four studied PMs, mostly deposits in the nasal cavity (see Figure S4 for details). In addition, biochar, i.e., the second most hydrophobic PM studied here, also demonstrates a significant amount of deposition in the nasal cavity and moderate deposition in trachea (see Figure S5 for detailed histology of PM-induced cilia damage). In contrast, no PM2.5 and dust, i.e., the two least hydrophobic PMs studied here, were found in the nasal and tracheal regions. Instead. PM2.5 and dust mostly deposit in the alveolar region of the lung (after 24 hours; see Figure S6 for detailed histology of PM-induced alveolar collapse and infiltration of inflammatory cells), while no carbon black particles were found in alveoli. It should be noted that more biochar particles were found in the alveoli than dust particles, which appears to be an outlier. Given that biochar is more hydrophobic than dust (Fig. 1), one would expect it to deposit less in the alveoli than dust. This anomaly may be attributed to the low-dose exposure model employed in this study, which is particularly sensitive to particles exhibiting extreme hydrophobicity and hydrophilicity.

Cytotoxicity and alveolar inflammatory responses induced by the PM

We have studied the *in vitro* cytotoxicity of the PMs, in a range of particle concentrations from 10 to 100 μ g/mL, using a commonly used human bronchial epithelial cell line (BEAS-2B). As shown in Fig. 4A, at

 Table 2

 Characterization of the particulate matter used in this study.

Particulate matter	PM2.5	Dust	Biochar	Carbon black
Morphology (Bar = 1 μm)				1 <u>µm</u>
Primary size distribu. Aerodynamic size (µm) Zeta potential (mV)	$\begin{array}{l} 300 \text{ nm} - 2 \mu\text{m} \\ 1.37 \pm 0.01 \\ \text{-}12.0 \pm 0.6 \end{array}$	500 nm $-$ 6 μ m 3.21 \pm 0.07 $-$ 16.6 \pm 0.3	$\begin{array}{l} 200 \text{ nm} - 3 \mu\text{m} \\ 1.46 \pm 0.02 \\ -29.8 \pm 0.1 \end{array}$	20 - 90 nm 1.20 ± 0.03 -23.1 ± 0.3

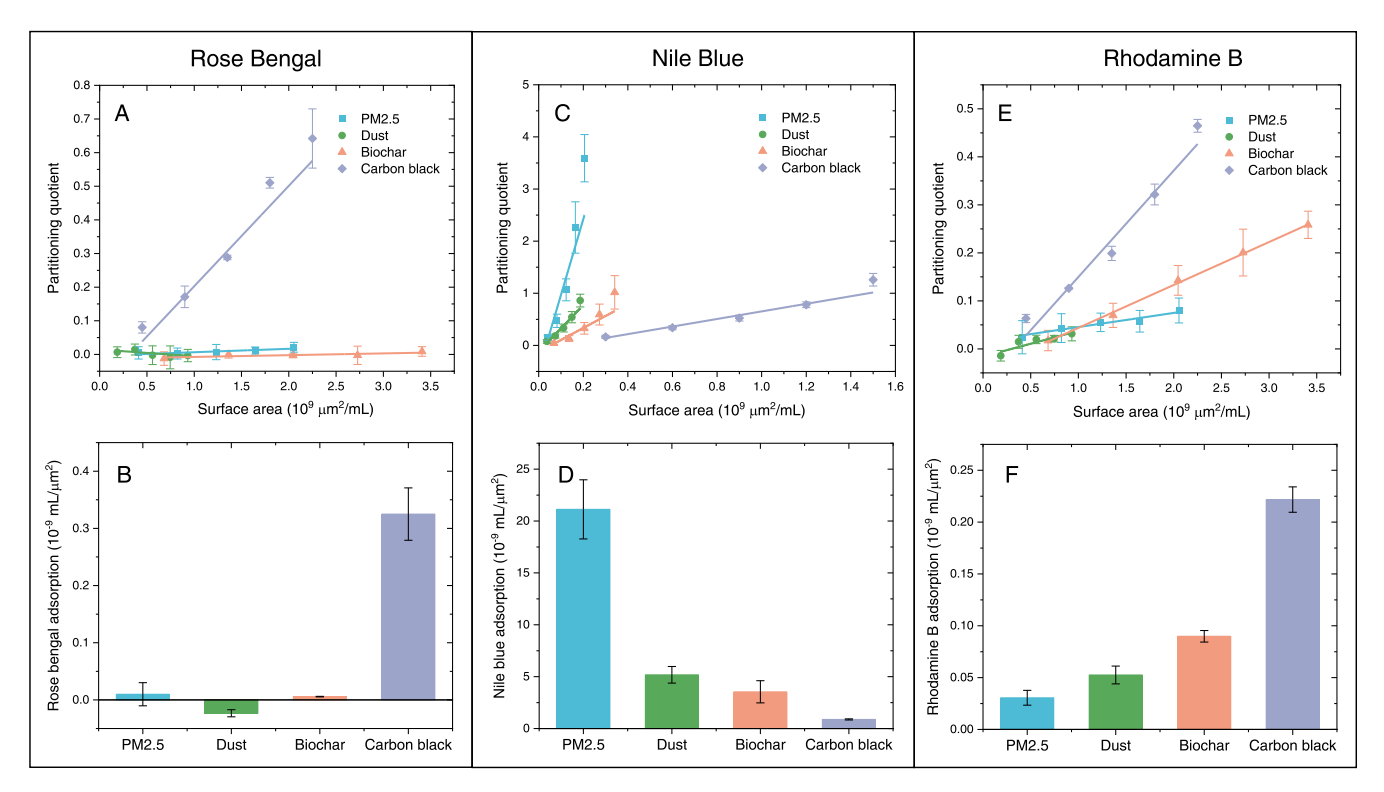


Fig. 1. Comparison of different dye partitioning methods to characterize the hydrophobicity/hydrophilicity of four PMs, *i.e.*, PM2.5, dust, biochar, and carbon black. **(A)** Linear regression of the partitioning quotient (PQ) of rose bengal (RB) against the surface areas of the PM. **(B)** RB adsorption, corresponding to the rank of hydrophobicity of the PM, determined from the slopes shown in panel A. **(C)** Linear regression of the PQ of nile blue (NB) against the surface areas of the PM. **(D)** NB adsorption, corresponding to the rank of hydrophilicity of the PM. p < 0.05 for comparison between any two PMs except for dust and biochar. **(E)** Linear regression of the PQ of rhodamine B (RhB) against the surface areas of the PM. **(F)** RhB adsorption, corresponding to the rank of hydrophobicity of the PM. p < 0.05 for comparison between any two PMs.

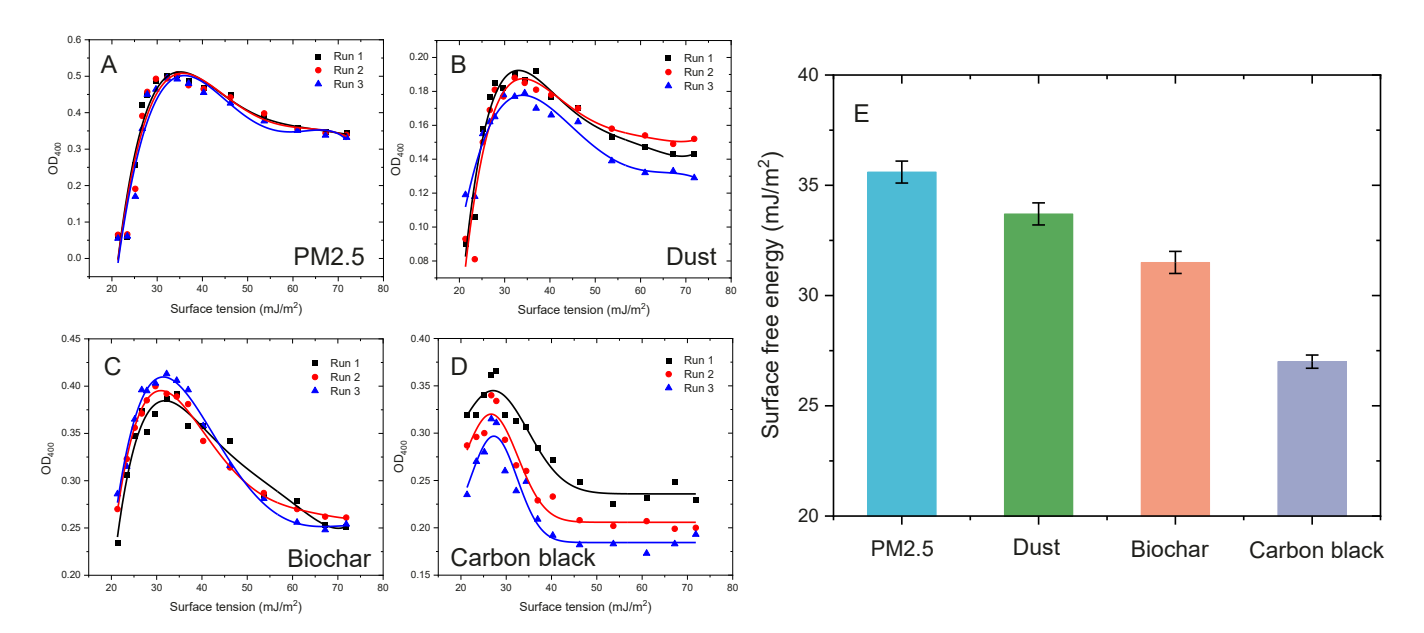
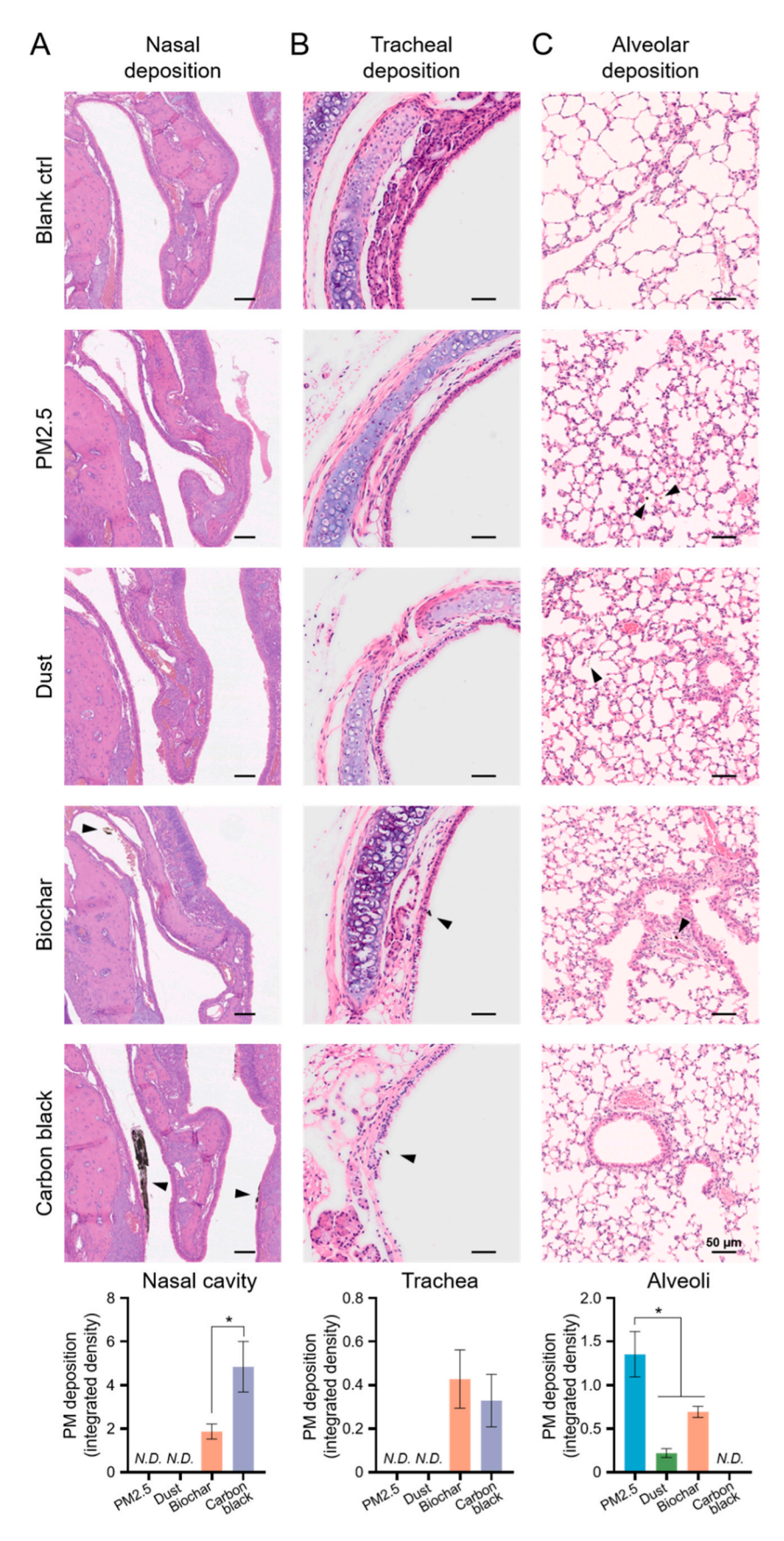


Fig. 2. Verification of the hydrophobicity measurements using the maximum particle dispersion (MPD) method. Each panel shows the optical density at 400 nm (OD₄₀₀) as a function of the surface tension of the probing liquids. The peak OD₄₀₀ value indicates that particles are maximally dispersed in a probing liquid of which the surface tension is equivalent to the surface free energy (SFE) of dispersed particles. Three runs of each measurement are presented to show reproducibility. (A) PM2.5, (B) dust, (C) biochar, and (D) carbon black. (E) The SFE of the PM determined with the MPD method. p < 0.05 for comparison between any two PMs. Based on the SFE measurements, the hydrophobicity of these PMs is ranked as PM2.5 (35.6 \pm 0.5 mJ/m²) < dust (33.7 \pm 0.5 mJ/m²) < biochar (31.5 \pm 0.5 mJ/m²) < carbon black (27.0 \pm 0.3 mJ/m²).



(caption on next page)

Fig. 3. Hematoxylin and eosin (H&E) stained histology of (A) the nasal cavity, (B) trachea, and (C) alveoli of mice with intranasal administration of PBS (blank control) or various particulate matters (PMs) at 1 mg/kg bodyweight, 2 hours (for A and B) and 24 hours (for C) after exposure. The stained sections show differential deposition of the PM, including PM2.5, dust, biochar, and carbon black, in the nasal, tracheal, and alveolar regions of the lung. Black arrowheads point to locally deposited PM. Bar = $50 \mu m$. The last row shows the quantitative analysis of the differential deposition of PM in the nasal cavity, trachea, and alveola, respectively. It was measured using the integrated density = area × mean intensity of the PM. N.D. = not detectable. * indicates p < 0.05.

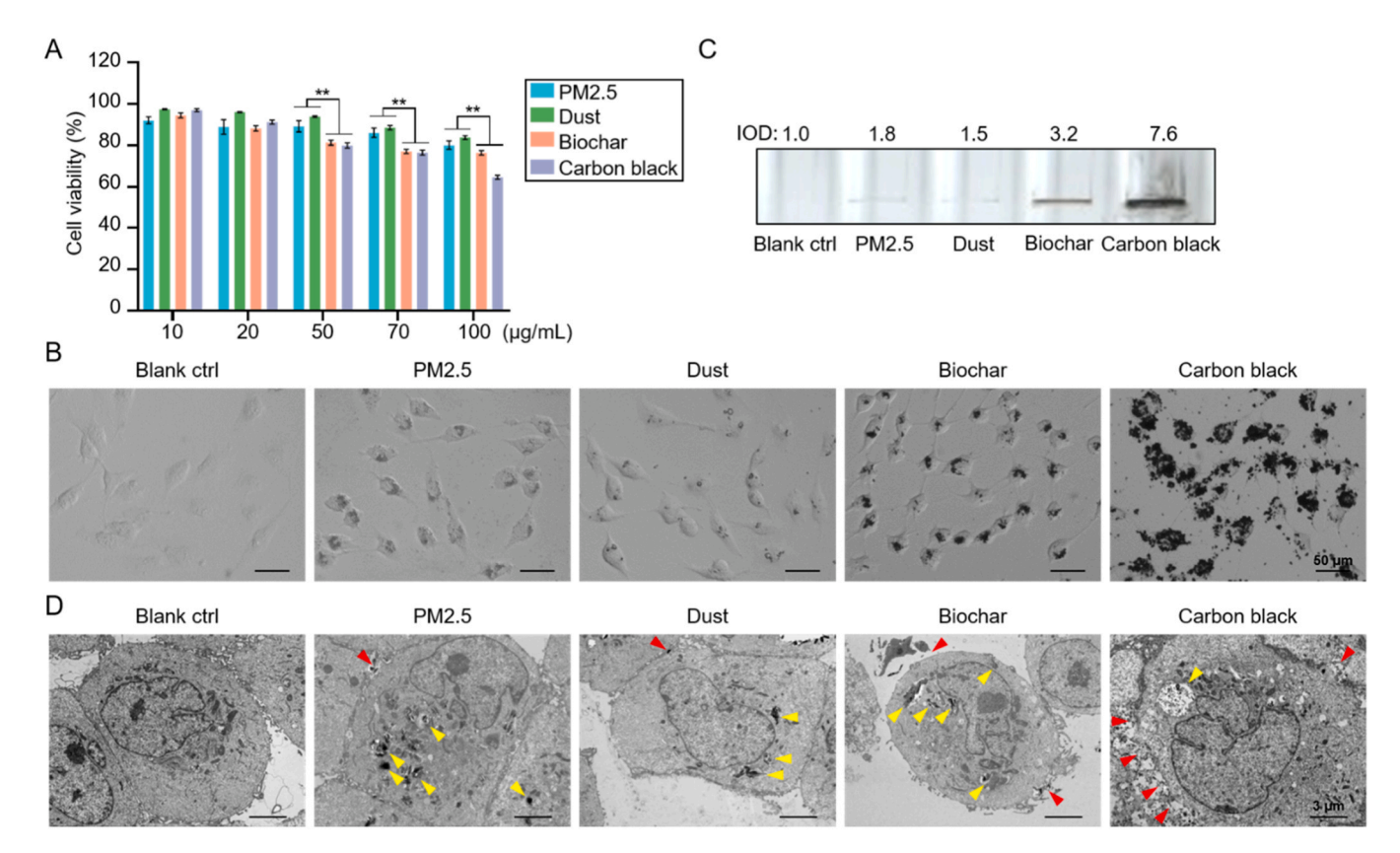


Fig. 4. *In vitro* cytotoxicity of the PM. **(A)** Viability of BEAS-2B cells upon exposure to various PMs, *i.e.*, PM2.5, dust, biochar, and carbon black, at 10, 20, 50, 70, and 100 μg/mL for 24 h (n = 6). ** indicates p < 0.001. **(B)** Representative phase-contrast images of BEAS-2B cells exposed to these PMs at 50 μg/mL for 24 h. Blank control: PBS only. Bar = 50 μm. **(C)** SDS-PAGE gel images of PM adhesion onto BEAS-2B cells at 50 μg/mL for 24 h. PM adhesion is quantified with the integrated optical densitometry (IOD). **(D)** Representative ultrastructure of BEAS-2B cells exposed to these PMs at 50 μg/mL for 24 h. Yellow arrowheads denote PMs in the cytoplasm, and red arrowheads indicate PMs associated with the plasma membrane of the cells. Blank control: PBS only. Bar = 3 μm.

low exposure concentrations, *i.e.*, 10 and 20 µg/mL, no statistically significant differences in cell viability were found among these PMs. When the exposure concentration was increased to 50 µg/mL and beyond (up to $100 \,\mu\text{g/mL}$), it was found that carbon black particles were significantly more toxic than PM2.5 and dust particles. Representative phase-contrast images of BEAS-2B cells illustrate a significant association of carbon black particles with their plasma membranes following exposure to 50 µg/mL PM for 24 hours (Fig. 4B). To validate these findings, an SDS-PAGE investigation was conducted to semi-quantify the PM attached to BEAS-2B cells based on the absorbance of each band. As depicted in Fig. 4C, it is evident that carbon black particles exhibit a considerably higher adhesion to the plasma membranes of PM-treated BEAS-2B cells compared to the other particles. This observation aligns well with the histological analysis presented in Fig. 3.

Fig. 4D shows the ultrastructure of the BEAS-2B cells 24 h after exposure to the PM. It was found that a majority of the PM2.5, dust, and biochar particles were internalized by the cells, while the carbon black particles were found to be primarily associated with the plasma membrane of the cells. The dynamics of the cellular internalization process was also studied with laser scanning confocal microscopy (LSCM) 6 and 24 h after exposure to the PM. As shown in Figure S7, 6 h after exposure, a majority of the PM was found to be localized at the plasma membrane of the BEAS-2B cells. After 24 h exposure, most PM2.5, dust, and biochar

particles were ingested into the BEAS-2B cells, except for the carbon black particles, which were found to be primarily accumulated at the plasma membrane of the cells.

We then studied the alveolar inflammatory responses induced by the PM with the hypothesis that the inflammatory responses are proportional to the amount of PM selectively deposited in the alveolar region. As shown in Fig. 5A, PM2.5, i.e., the most hydrophilic PM tested here, induced the highest alveolar inflammation level, indicated by the most infiltrated inflammatory cells, including the alveolar macrophages (AM), monocytes (MO), and dendritic cells (DC). The carbon black, i.e., the most hydrophobic PM tested here, induced the least alveolar inflammation. Fig. 5B shows the systematic inflammatory reactions in response to different PMs. The peripheral blood of mice treated with PM2.5, dust, and biochar shows a significant increase of the neutrophil (NE) count and the neutrophil-to-lymphocyte (NE/LY) ratio, 24 hours after exposure to the PM. The inflammatory phenotypes were restored to nearly normal levels within 72 hours. These in vitro and in vivo data collectively support the hypothesis that the hydrophobicity of PM mediates its lung deposition, thus regulating local and systematic inflammatory reactions after exposure to these PMs.

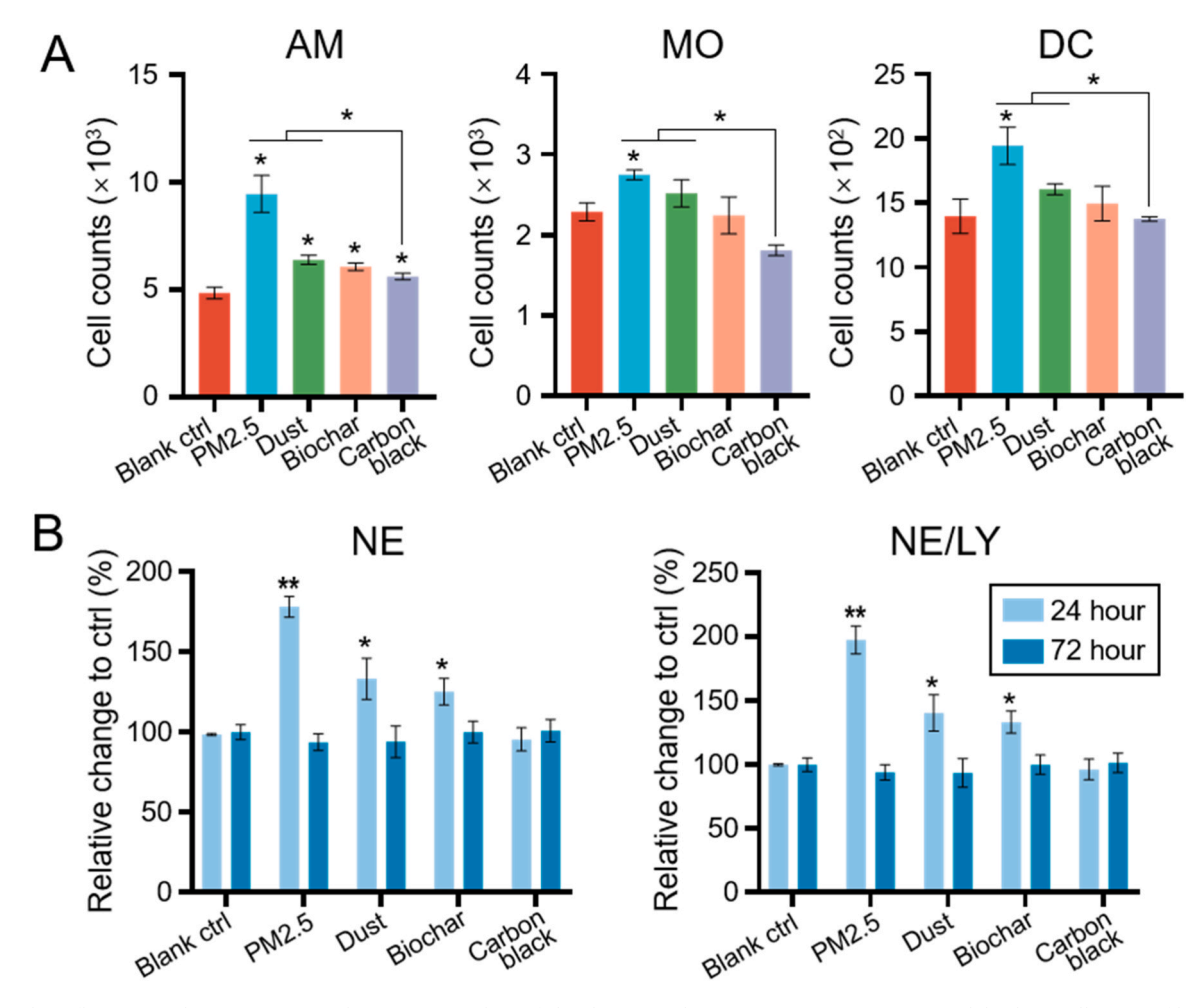


Fig. 5. Alveolar inflammation due to exposure to the PM. **(A)** Numbers of alveolar macrophages (AM), monocytes (MO), and dendritic cells (DC) infiltrated into the lung tissues, determined by flow cytometry 24 hours after intranasally treated with PBS (blank control) or the PM at 200 μ g/kg bodyweight (n = 4). **(B)** Relative changes of neutrophils (NE) and the ratio of neutrophils/lymphocytes (NE/LY) in the peripheral blood of mice at 24 and 72 hours after treated with PBS (blank control) or the PM (n = 5). * indicates p < 0.05, and ** indicates p < 0.001.

Discussion

It has long been accepted that the regional deposition of airborne PM in the respiratory system is predominantly influenced by the aero-dynamic size of the particles [14,15]. PM within the size range of 0.5 and 5 μm is most likely to deposit in the alveolar region, while particles larger than 5 μm are mostly trapped in the nasopharyngeal and the tracheobronchial regions. These larger particles are then cleared through mucociliary interactions, eventually being either coughed out or swallowed [9,13].

The PMs studied here, with an aerodynamic size ranging from 1.2 to 3.2 µm (Table 2), are presumed to undergo deposition primarily through gravitational sedimentation[9,10]. Despite having similar aerodynamic sizes, these PMs exhibit distinct regional deposition patterns in the respiratory tract. Carbon black particles tend to be predominantly trapped in the nasal cavity, whereas biochar particles show a propensity for deposition in the trachea. In contrast, PM2.5 and dust particles penetrate deep into the alveoli (Fig. 3). Correlation analysis suggests that the deposition of PM in the nasal cavity is positively correlated with the RhB adsorption (p < 0.05), and is negatively correlated with the surface free energy of these PMs (p < 0.05) (Figure S8A). In general, an opposite dependence is found for particle deposition in the lung alveoli although no statistical significance is determined (Figure S8B). Other physicochemical properties, including the particle size, surface area, pore volume, and zeta potential, showed no significant correlations with the behavior of particle deposition. These observations suggest that the

hydrophobicity of these PMs plays a significant role in mediating their deposition within the lungs.

It is important to note that the concepts of "hydrophobicity" and "hydrophilicity" as used in this paper are relative terms. Traditional definitions of hydrophobic and hydrophilic surfaces, typically based on water contact angle measurements, have been shown to lack a consistent rationale [46]. In this study, the hydrophobicity and hydrophilicity of PM are determined to provide a quantitative measure of its relative affinity to water. Considering the high surface free energy or surface tension of water, a hydrophobic PM is expected to possess a low surface free energy, whereas a hydrophilic PM is expected to possess a relatively high surface free energy [26,27].

In this study, we used a mouse model with intranasal administration of PM, rather than intratracheal administration. Mammalian respiratory tracts comprise upper and lower divisions. The upper tract includes the nose, nasal cavities, pharynx and a portion of the larynx, while the lower tract encompasses the trachea, bronchi, bronchioles and alveoli. Intratracheal administration of PM bypasses the upper respiratory tract, thereby hindering the investigation of PM deposition in the upper tract, especially the nasal cavity [47]. Studies have shown that lung deposition of PM via intranasal administration is less than one third of that achieved through intratracheal instillation [48]. Despite the lower lung deposition, recent research has concluded that intranasal exposure is comparably effective to intratracheal exposure in a mouse model of acute respiratory distress syndrome (ARDS) induced by single lipopolysaccharide exposure [49]. Based on this evidence, we selected

intranasal administration of PM as a low-dose exposure model with greater environmental relevance.

Detecting regional particle deposition in the lungs presents a significant experimental challenge in low-dose exposure models. Besides numerical modeling, such as those outlined by the international commission on radiological protection (ICRP) model or the multiple-path particle dosimetry (MPPD) model, only a few experimental techniques are available for direct detection of particle deposition in lung tissues [50]. To the best of our knowledge, these experimental methods primarily include optical or electron microscopy to observe particles deposited in lung tissues and gamma scintigraphy utilizing radiolabeled particles [51]. Among these options, we opted for bright-field optical microscopy (Fig. 3) due to its simplicity, label-free nature, and specificity in assessing regional particle deposition in the lungs.

Previous studies involving particles with extreme hydrophobic and hydrophilic characteristics have qualitatively demonstrated that the hydrophobicity of PM can impact its lung deposition. The hygroscopic growth of hydrophilic particles in the respiratory tract is identified as a crucial factor influencing their regional deposition[52–54]. Notably, investigations using titanium dioxide (TiO₂) nanoparticles, with various surface modifications, have been employed to explore the relationship between particle hydrophobicity and lung deposition[55–57]. Results from these studies indicate that hydrophilic, pristine TiO₂ nanoparticles triggered significantly greater inflammatory responses in lung alveoli compared to hydrophobic, surface-modified TiO₂ nanoparticles [55–57].

In this study, a similar pattern emerges, with the least hydrophobic PM, *i.e.*, PM2.5, resulting in the highest level of alveolar inflammation (Fig. 5). It is essential to highlight that, despite PM2.5 inducing the most significant alveolar inflammation (Fig. 5), it exhibits the least toxicity to lung cells *in vitro* (Fig. 4). This observation aligns with the prevailing consensus that the cytotoxicity of nanoparticles increases with higher particle hydrophobicity[58–66]. Collectively, these findings suggest that PM2.5 induces alveolar inflammation by preferentially depositing in the alveolar region compared to other tested PMs. The differential lung deposition of PM appears to be regulated by its hydrophobicity.

Conclusions

In conclusion, we have developed a novel nonionic dye partitioning method to quantitatively characterize the hydrophobicity of PM. The use of a nonionic dye, rhodamine B, eliminates experimental artifacts arising from unwanted dye adsorption due to electrostatic interactions, thus significantly increasing the accuracy and applicability of the method. Our study revealed that the lung deposition of four types of PM originated from common anthropogenic sources, including PM2.5, dust, biochar, and carbon black, is mediated by their hydrophobicity. The most hydrophobic PM tends to be trapped in the nasal region, while the least hydrophobic PM penetrates deep into the alveoli, leading to severe lung inflammation. The hydrophobicity-dependent deposition of PM in the respiratory tract offers valuable insights into understanding the acute lung toxicity of inhaled PM, the pathogenic mechanisms of virusladen particles, and the design of safer and more efficacious inhalable nanomedicines. Furthermore, the nonionic dye partitioning method shows promise as a user-friendly and cost-effective approach for characterizing the hydrophobicity of PM.

CRediT authorship contribution statement

Juan Ma: Writing – review & editing, Supervision, Resources, Project administration, Funding acquisition, Conceptualization. Yi Y. Zuo: Writing – review & editing, Supervision, Resources, Project administration, Funding acquisition, Conceptualization. Sijin Liu: Writing – review & editing, Supervision, Resources, Project administration, Funding acquisition. Guangle Li: Writing – original draft, Validation, Methodology, Investigation, Data curation. Zheng Dong: Writing – original draft, Validation, Methodology, Investigation, Data

curation. **Quanzhong Ren:** Methodology. **Bingbing Sun:** Writing – review & editing, Resources.

Declaration of Competing Interest

The authors declare that they have no known competing financial interests or personal relationships that could have appeared to influence the work reported in this paper.

Data Availability

Data will be made available on request.

Acknowledgments

This work was supported by the National Science Foundation (grant number CBET-2011317) to Y.Y.Z., the National Natural Science Foundation of China (grant number 22076210) and the Youth Innovation Promotion Association of Chinese Academy of Science (grant number 2022042) to J.M., and the National Natural Science Foundation of China (grant number 22150006, 21920102007) to S.J.L.

Appendix A. Supporting information

Supplementary data associated with this article can be found in the online version at doi:10.1016/j.nantod.2024.102360.

References

- [1] P.K. Hopke, Q. Dai, L. Li, Y. Feng, Sci. Total Environ. 740 (2020) 140091.
- [2] K.R. Daellenbach, G. Uzu, J. Jiang, L.-E. Cassagnes, Z. Leni, A. Vlachou, G. Stefenelli, F. Canonaco, S. Weber, A. Segers, J.J.P. Kuenen, M. Schaap, O. Favez, A. Albinet, S. Aksoyoglu, J. Dommen, U. Baltensperger, M. Geiser, I. El Haddad, J.-L. Jaffrezo, A.S.H. Prévôt, Nature 587 (2020) 414–419.
- [3] G. Oberdörster, E. Oberdörster, J. Oberdörster, Environ. Health Perspect. 113 (2005) 823–839.
- [4] A. Valavanidis, K. Fiotakis, T. Vlachogianni, J. Environ. Sci. Health, Part C. 26 (2008) 339–362.
- [5] E.M. Quezada-Maldonado, Y. Sánchez-Pérez, Y.I. Chirino, C.M. García-Cuellar, Environ. Pollut. 287 (2021) 117313.
- [6] Z. Dong, J. Ma, J. Qiu, Q. Ren, Q. Shan, X. Duan, G. Li, Y.Y. Zuo, Y. Qi, Y. Liu, G. Liu, I. Lynch, M. Fang, S. Liu, Sci. Adv. 9 (2023) eadf2165.
- [7] K.-H. Kim, E. Kabir, S. Kabir, Environ. Int. 74 (2015) 136-143.
- [8] K.E. Cosselman, A. Navas-Acien, J.D. Kaufman, Nat. Rev. Cardiol. 12 (2015) 627–642.
- [9] G. Li, D. Liu, Y.Y. Zuo, Nano-bio Interactions in the Lung, in: N. Gu (Ed.), Nanomedicine, Springer Nature Singapore, Singapore, 2023, pp. 469–499.
- [10] J. Heyder, Proc. Am. Thorac. Soc. 1 (2004) 315-320.
- [11] Y.Y. Zuo, W.E. Uspal, T. Wei, ACS Nano 14 (2020) 16502–16524.
- [12] Y. Guo, Y. Ma, X. Chen, M. Li, X. Ma, G. Cheng, C. Xue, Y.Y. Zuo, B. Sun, ACS Nano 17 (2023) 2813–2828.
- [13] C.A. Ruge, J. Kirch, C.M. Lehr, Lancet Respir. Med. 1 (2013) 402–413.
- [14] T.C. Carvalho, J.I. Peters, R.O. Williams, 3rd, International journal of pharmaceutics. 406 (2011) 1-10.
- [15] W.C. Hinds, Aerosol Technology: Properties, Behavior, and Measurement of Airborne Particles, Wiley, Hoboken, NJ, 1999.
- [16] M.-C. Jones, S.A. Jones, Y. Riffo-Vasquez, D. Spina, E. Hoffman, A. Morgan, A. Patel, C. Page, B. Forbes, L.A. Dailey, J. Control. Release 183 (2014) 94–104.
- [17] A. Voliotis, C. Samara, Environ. Sci. Pollut. Res. 25 (2018) 33724–33735.
- [18] C.-X. Tang, Y. Dong, X.-Y. Yuan, R. Wang, C.-C. Wu, L.-J. Bao, E.Y. Zeng, Sci. Total Environ. 889 (2023) 164225.
- [19] G. Azimi, R. Dhiman, H.-M. Kwon, A.T. Paxson, K.K. Varanasi, Nat. Mater. 12 (2013) 315–320.
- [20] K. Grundke, A. Augsburg, J. Adhes. Sci. Technol. 14 (2000) 765-775.
- [21] Y. Xiao, M.R. Wiesner, J. Hazard. Mater. 215-216 (2012) 146-151.
- [22] C.T. Jafvert, P.P. Kulkarni, Environ. Sci. Technol. 42 (2008) 5945–5950.
- [23] R.H. Müller, D. Rühl, M. Lück, B.R. Paulke, Pharm. Res. 14 (1997) 18-24.
- [24] G. Li, K.K.H.Y. Ho, Y.Y. Zuo, J. Phys. Chem. C. 126 (2022) 832–837.
- [25] S. Mohammadi-Jam, K.E. Waters, Adv. Colloid Interface Sci. 212 (2014) 21–44.
- [26] Z. Cao, S.N. Tsai, Y.Y. Zuo, Anal. Chem. 91 (2019) 12819–12826.
- [27] G. Li, Z. Cao, K.K.H.Y. Ho, Y.Y. Zuo, Anal. Chem. 94 (2022) 2078–2086.
- [28] R.P. Valle, C.L. Huang, J.S.C. Loo, Y.Y. Zuo, ACS Sustain. Chem. Eng. 2 (2014) 1574–1580.
- [29] J. Ma, X. Liu, Y. Yang, J. Qiu, Z. Dong, Q. Ren, Y.Y. Zuo, T. Xia, W. Chen, S. Liu, ACS Nano 15 (2021) 9717–9731.

- [30] V.R. Batistela, D.S. Pellosi, F.D. de Souza, W.F. da Costa, S.M. de Oliveira Santin, V. R. de Souza, W. Caetano, H.P.M. de Oliveira, I.S. Scarminio, N. Hioka, Spectrochim. Acta Part A: Mol. Biomol. Spectrosc. 79 (2011) 889–897.
- [31] C.-W. Lin, J.R. Shulok, Y.-K. Wong, C.F. Schanbacher, L. Cincotta, J.W. Foley, Cancer Res. 51 (1991) 1109–1116.
- [32] M. Beija, C.A.M. Afonso, J.M.G. Martinho, Chem. Soc. Rev. 38 (2009) 2410-2433.
- [33] H.N. Kim, M.H. Lee, H.J. Kim, J.S. Kim, J. Yoon, Chem. Soc. Rev. 37 (2008) 1465–1472.
- [34] L. Yuan, W. Lin, K. Zheng, S. Zhu, Acc. Chem. Res. 46 (2013) 1462-1473.
- [35] R.W. Ramette, E.B. Sandell, J. Am. Chem. Soc. 78 (1956) 4872–4878.
- [36] I.L. Arbeloa, K.K. Rohatgi-Mukherjee, Chem. Phys. Lett. 128 (1986) 474–479.
- [37] I. Rosenthal, P. Peretz, K.A. Muszkat, J. Phys. Chem. 83 (1979) 350–353.
- [38] I.L. Arbeloa, P.R. Ojeda, Chem. Phys. Lett. 79 (1981) 347–350.
- [39] V. Kumar, M. Singh, K. Behera, S. Pandey, J. Mol. Liq. 319 (2020) 114195.
- [40] S. Rossi, F. Herbrik, S. Resta, A. Puglisi, Molecules 27 (2022) 5096.
- [41] I. Moreno-Villoslada, M. Jofré, V. Miranda, R. González, T. Sotelo, S. Hess, B. L. Rivas, J. Phys. Chem. B 110 (2006) 11809–11812.
- [42] C.A. Wakeman, J.L. Moore, M.J. Noto, Y. Zhang, M.D. Singleton, B.M. Prentice, B. A. Gilston, R.S. Doster, J.A. Gaddy, W.J. Chazin, R.M. Caprioli, E.P. Skaar, Nat. Commun. 7 (2016) 11951.
- [43] E.R. Summerbell, J.K. Mouw, J.S.K. Bell, C.M. Knippler, B. Pedro, J.L. Arnst, T. O. Khatib, R. Commander, B.G. Barwick, J. Konen, B. Dwivedi, S. Seby, J. Kowalski, P.M. Vertino, A.I. Marcus, Sci. Adv. 6 (2020) eaaz6197.
- [44] A.V. Misharin, L. Morales-Nebreda, G.M. Mutlu, G.R. Budinger, H. Perlman, Am. J. Respir. Cell Mol. Biol. 49 (2013) 503–510.
- [45] J. Ma, R. Liu, X. Wang, Q. Liu, Y. Chen, R.P. Valle, Y.Y. Zuo, T. Xia, S. Liu, ACS Nano 9 (2015) 10498–10515.
- [46] K.-Y. Law, J. Phys. Chem. Lett. 5 (2014) 686-688.
- [47] A.L. Linderholm, L.M. Franzi, K.J. Bein, K.E. Pinkerton, J. A. Last (2015).
- [48] L. Wu, C. Rodríguez-Rodríguez, D. Cun, M. Yang, K. Saatchi, U.O. Häfeli, Eur. J. Pharm. Biopharm.: Off. J. Arb. fur Pharm. Verfahr. e. V. 152 (2020) 108–115.

- [49] F. Khadangi, A.-S. Forgues, S. Tremblay-Pitre, A. Dufour-Mailhot, C. Henry, M. Boucher, M.-J. Beaulieu, M. Morissette, L. Fereydoonzad, D. Brunet, A. Robichaud, Y. Bossé, Sci. Rep. 11 (2021) 7777.
- [50] J. Löndahl, W. Möller, J.H. Pagels, W.G. Kreyling, E. Swietlicki, O. Schmid, J. Aerosol Med. Pulm. Drug Deliv. 27 (2014) 229–254.
- [51] M.F. Biddiscombe, S.N. Meah, S.R. Underwood, O.S. Usmani, J. Aerosol Med. Pulm. Drug Deliv. 24 (2011) 165–173.
- [52] K.W. Tu, E.O. Knutson, Aerosol Sci. Technol. 3 (1984) 453-465.
- [53] K. Kademoglou, G. Giovanoulis, A. Palm-Cousins, J.A. Padilla-Sanchez, J. Magnér, C.A. de Wit, C.D. Collins, Environ. Sci. Technol. Lett. 5 (2018) 329–334.
- [54] Á. Farkas, P. Füri, W. Thén, I. Salma, Sci. Total Environ. 806 (2022) 151202.
- [55] G. Oberdörster, Int. Arch. Occup. Environ. Health 74 (2000) 1-8.
- [56] D.B. Warheit, K.L. Reed, T.R. Webb, Exp. Lung Res. 29 (2003) 593-606.
- [57] B. Rehn, F. Seiler, S. Rehn, J. Bruch, M. Maier, Toxicol. Appl. Pharmacol. 189 (2003) 84–95.
- [58] S.T. Kim, K. Saha, C. Kim, V.M. Rotello, Acc. Chem. Res. 46 (2013) 681-691.
- [59] A. Chompoosor, K. Saha, P.S. Ghosh, D.J. Macarthy, O.R. Miranda, Z.J. Zhu, K. F. Arcaro, V.M. Rotello, Small (Weinh. der Bergstr., Ger.) 6 (2010) 2246–2249.
- [60] H. Yin, H.P. Too, G.M. Chow, Biomaterials 26 (2005) 5818-5826.
- [61] Y.W. Chun, W. Wang, J. Choi, T.-H. Nam, Y.-H. Lee, K.-K. Cho, Y.-M. Im, M. Kim, Y.-H. Gwon, S.S. Kang, J.D. Lee, K. Lee, D. Khang, T.J. Webster, Carbon 49 (2011) 2002, 2103
- [62] D.F. Moyano, M. Goldsmith, D.J. Solfiell, D. Landesman-Milo, O.R. Miranda, D. Peer, V.M. Rotello, J. Am. Chem. Soc. 134 (2012) 3965–3967.
- [63] S. Li, S. Zhai, Y. Liu, H. Zhou, J. Wu, Q. Jiao, B. Zhang, H. Zhu, B. Yan, Biomaterials 52 (2015) 312–317.
- [64] C.R. Anderson, Y.D.M. Gnopo, F. Gambinossi, S.E. Mylon, J.K. Ferri, J. Biomed. Mater. Res. Part A 106 (2018) 1061–1071.
- [65] H. Sun, C. Jiang, L. Wu, X. Bai, S. Zhai, Front. Bioeng. Biotechnol. 7 (2019) 414.
- [66] F. Liu, S. Li, H. Feng, L. Li, T. Yue, B. Yan, Environ. Sci.: Nano 8 (2021) 3746-3761.